Nuclear Star Cluster formation by the first generation globular clusters disruption

2026 Fberuary 4

Dr. Sci. Peter Berczik

MAO, National Academy of Sciences of Ukraine, Kiev.
CAMK, Polish Academy of Sciences, Warsaw, Poland.

2023 Sept. +3 years

PAN.BFB.S.BWZ.329.022.2023

JÜLICH Forschungszentrum | JÜLICH SUPERCOMPUTING CENTRE

Formation and evolution of the Nuclear Star Cluster in the Milky Way and other spiral galaxies on the cosmological time scale.

PAN.BFB.S.BWZ.329.022.2023

Dr. Maryna Ishchenko
MAO, NASU
Warsaw / Kyiv

PhD student Margaryta Sobolenko
MAO, NASU
Warsaw / Kyiv

Dr. Oleksandr Veles
MAO, NASU
Kyiv / Warsaw

PhD student Olexander Sobodar
MAO, NASU
Kyiv / Warsaw

- **Peter Berczik**
- **Main Astronomical Observatory, National Academy of Sciences of Ukraine**
- **Nicolaus Copernicus Astronomical Centre of the Polish Academy of Sciences**

During the project (Sep. 2023): 23 ref. publications

A&A	18
MNRAS	3
ApJ	2

Total citations: 207 in 143 papers

April 14, 2023

Milky Way globular clusters on cosmological timescales. I. Evolution of the orbital parameters in time-varying potentials

Maryna Ishchenko[1,2], Margaryta Sobolenko[1], Peter Berczik[3,4,1,2], Sergey Khoperskov[5,6], Chingis Omarov[2], Olexander Sobodar[1], and Maxim Makukov[2]

Milky Way globular clusters on cosmological timescales. II. Interaction with the Galactic centre

April 10, 2023

Maryna Ishchenko[1,2], Margaryta Sobolenko[1], Dana Kuvatova[2], Taras Panamarev[3,2], and Peter Berczik[4,5,2,1]

7 August 2023

Milky Way globular clusters on cosmological timescales. III. Rates of interactions with each other

Maryna Ishchenko[1,2], Margaryta Sobolenko[1], Peter Berczik[3,4,1,2], Chingis Omarov[2], Olexander Sobodar[1], and Denis Yurin[2]

14 December 2023

Milky Way globular clusters on cosmological timescales

IV. Guests in the outer Solar System

Maryna Ishchenko[1,2,3], Peter Berczik[1,2,3,4], and Margarita Sobolenko[1,2]

Dynamical evolution of Milky Way globular clusters on the cosmological timescale

10 June 2024

I. Mass loss and interaction with the nuclear star cluster

Maryna Ishchenko[1,2,3,⋆], Peter Berczik[2,3,8,1], Taras Panamarev[7,3], Dana Kuvatova[3], Mukhagali Kalambay[3,4,5,6], Anton Gluchshenko[3], Oleksandr Veles[1,2], Margaryta Sobolenko[1,2], Olexander Sobodar[1,2], and Chingis Omarov[3]

Evolution of the disky second generation of stars in globular clusters on cosmological timescales

Peter Berczik[1,2,3,4,⋆], Taras Panamarev[5,4], Maryna Ishchenko[1,2,4], and Bence Kocsis[5]

2 January 2025

MAO, Kiev 8 node GPU cluster

MAO 4+4 new nodes 4xGF 2080S + 4xGF 3070 + 4xGF 4080

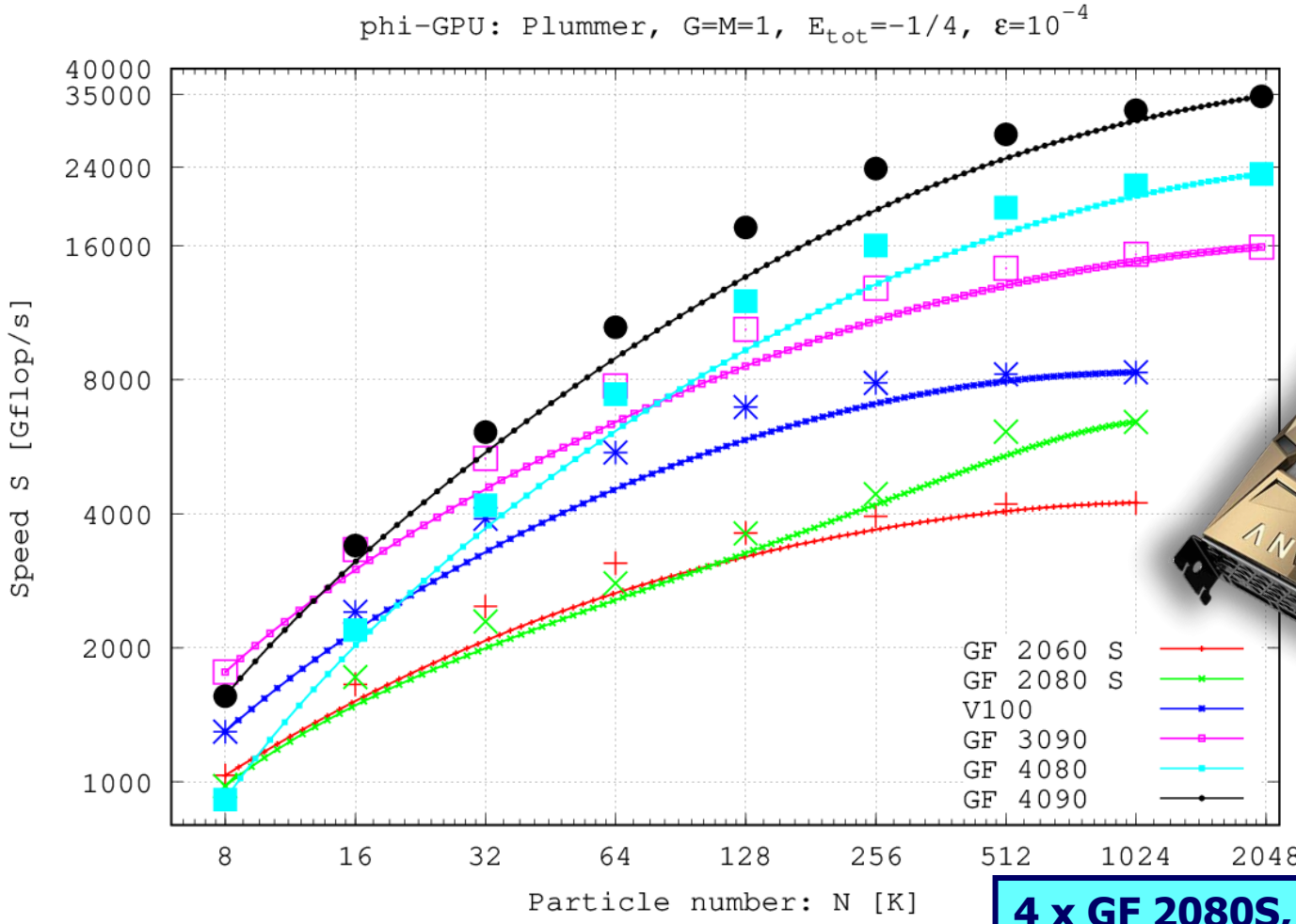

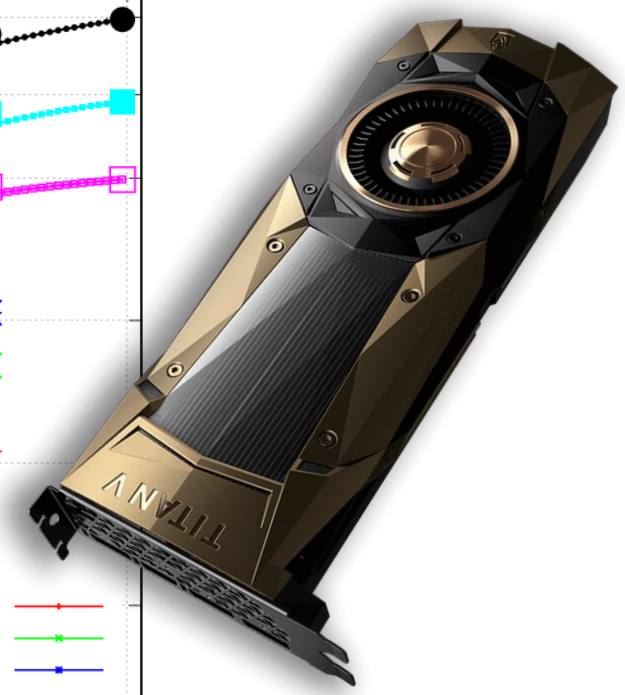

4 x GF 2080S, 3072 SP @ 1.81 GHz
4 x GF 3070, 5888 SP @ 1.77 GHz
4 x GF 4080, 9728 SP @ 2.54 GHz

JUWELS Booster consists of 936 compute nodes, each equipped with 4 NVIDIA A100 GPUs. The GPUs are hosted by AMD EPYC Rome CPUs. The compute nodes are connected with HDR-200 InfiniBand in a DragonFly+ topology.

The InfiniBand network of JUWELS Booster is implemented as a DragonFly+ network.

48 nodes are combined in a switch group (*cell*), interconnected in a full fat-tree topology, with 10 leaf switches and 10 spine switches in a two-level configuration. 40 Tbit/s of bi-section bandwidth is available.

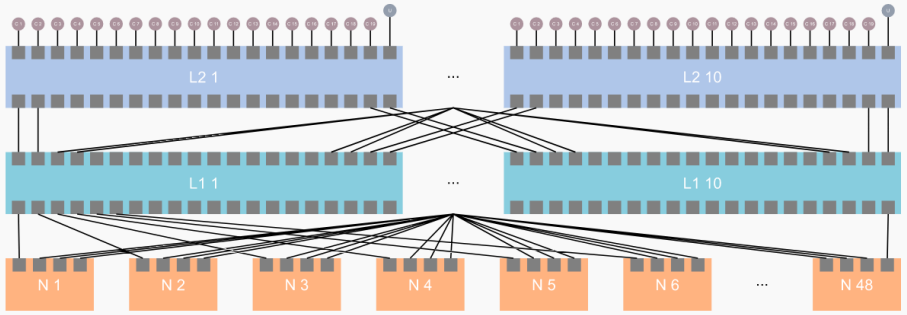

Sketch of the network topology within a JUWELS Booster cell with 48 nodes (`N1` to `N 48`), 10 level 1 switches (`L1 1` to `L1 10`) and 10 level 2 switches (`L2 1` to `L2 10`). Only a small subset of the total amount of links are shown for readability. The purple, 20th link leaving each level 2 switch should indicate the connection to JUWELS Cluster, while the other 19 outgoing level 2 links connect to other cells.

The configuration of JUWELS Booster compute nodes is the following

- **CPU**: AMD EPYC 7402 processor; 2 sockets, 24 cores per socket, SMT-2 (total: 2×24×2 = 96 threads) in NPS-4 [1] configuration (details on WikiChip)
- **Memory**: 512 GB DDR4-3200 RAM (of which at least 20 GB is taken by the system software stack, including the file system); 256 GB per socket; 8 memory channels per socket (2 channels per NUMA domain)
- **GPU**: 4 × NVIDIA A100 Tensor Core GPU with 40 GB; connected via NVLink3 to each other
- **Network**: 4 × Mellanox HDR200 InfiniBand ConnectX 6 (200 Gbit/s each), *HCA*
- **Periphery**: CPU, GPU, and network adapter are connected via 2 PCIe Gen 4 switches with 16 PCIe lanes going to each device (CPU socket: 2×16 lanes). PCIe switches are configured in *synthetic mode*.

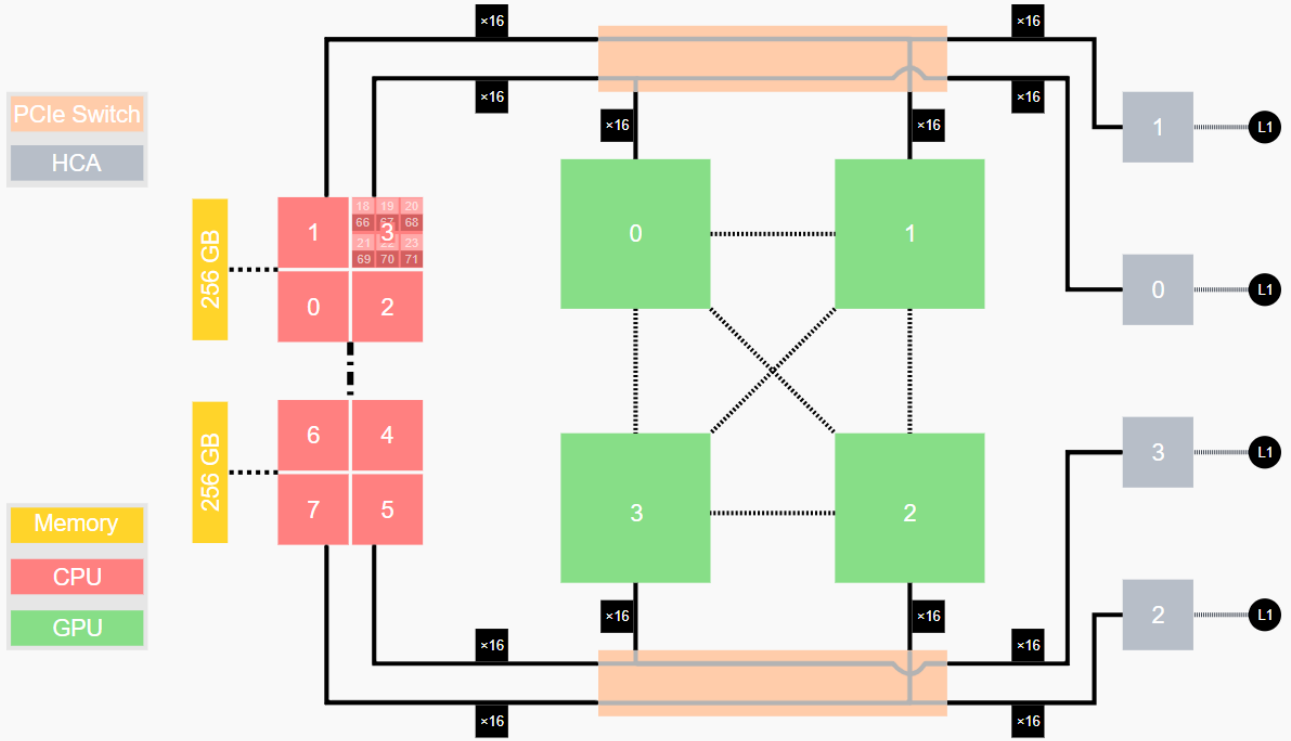

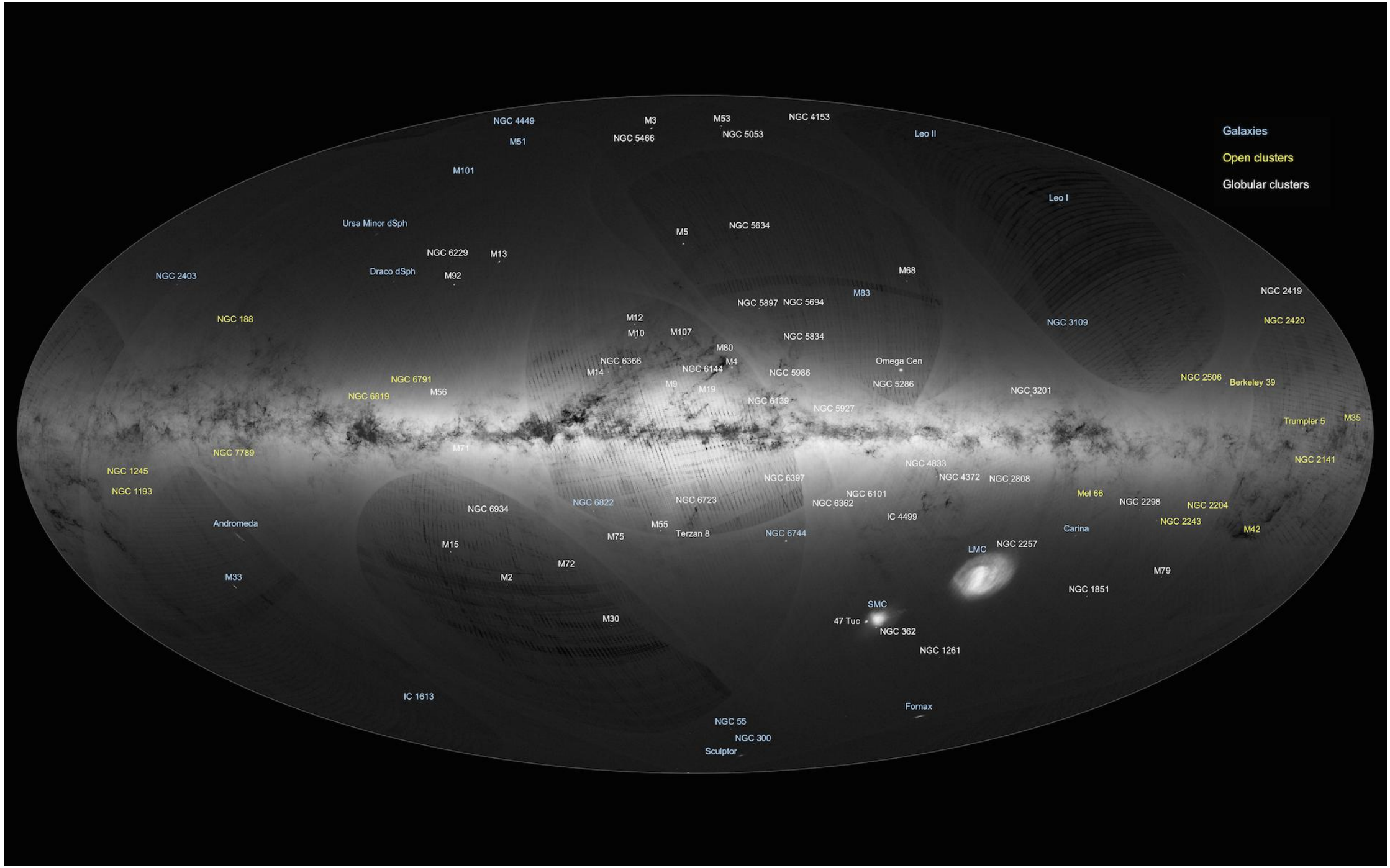
Galaxies
Open clusters
Globular clusters
NGC 4449
M3
M53
NGC 4153
M51
NGC 5466
NGC 5053
Leo II
M101
Leo I
Ursa Minor dSph
M5
NGC 5634
NGC 6229
M13
NGC 2403
Draco dSph
M92
M68
M83
NGC 2419
NGC 5897
NGC 5694
NGC 188
M12
NGC 3109
NGC 2420
M10
M107
NGC 5834
M80
NGC 6366
M4
Omega Cen
M14
NGC 6144
NGC 5986
NGC 6791
NGC 5286
NGC 2506
Berkeley 39
M9
M19
NGC 6819
M56
NGC 6139
NGC 3201
NGC 5927
Trumpler 5
M35
M71
NGC 7789
NGC 4833
NGC 2141
NGC 1245
NGC 6397
NGC 4372
NGC 2808
NGC 1193
NGC 6101
Mel 66
NGC 6822
NGC 6723
NGC 6362
NGC 2298
NGC 2204
NGC 6934
IC 4499
Andromeda
M55
NGC 2243
Carina
M42
M75
Terzan 8
NGC 6744
M15
LMC
NGC 2257
M72
M79
M33
M2
NGC 1851
SMC
M30
47 Tuc
NGC 362
NGC 1261
IC 1613
Fornax
NGC 55
NGC 300
Sculptor

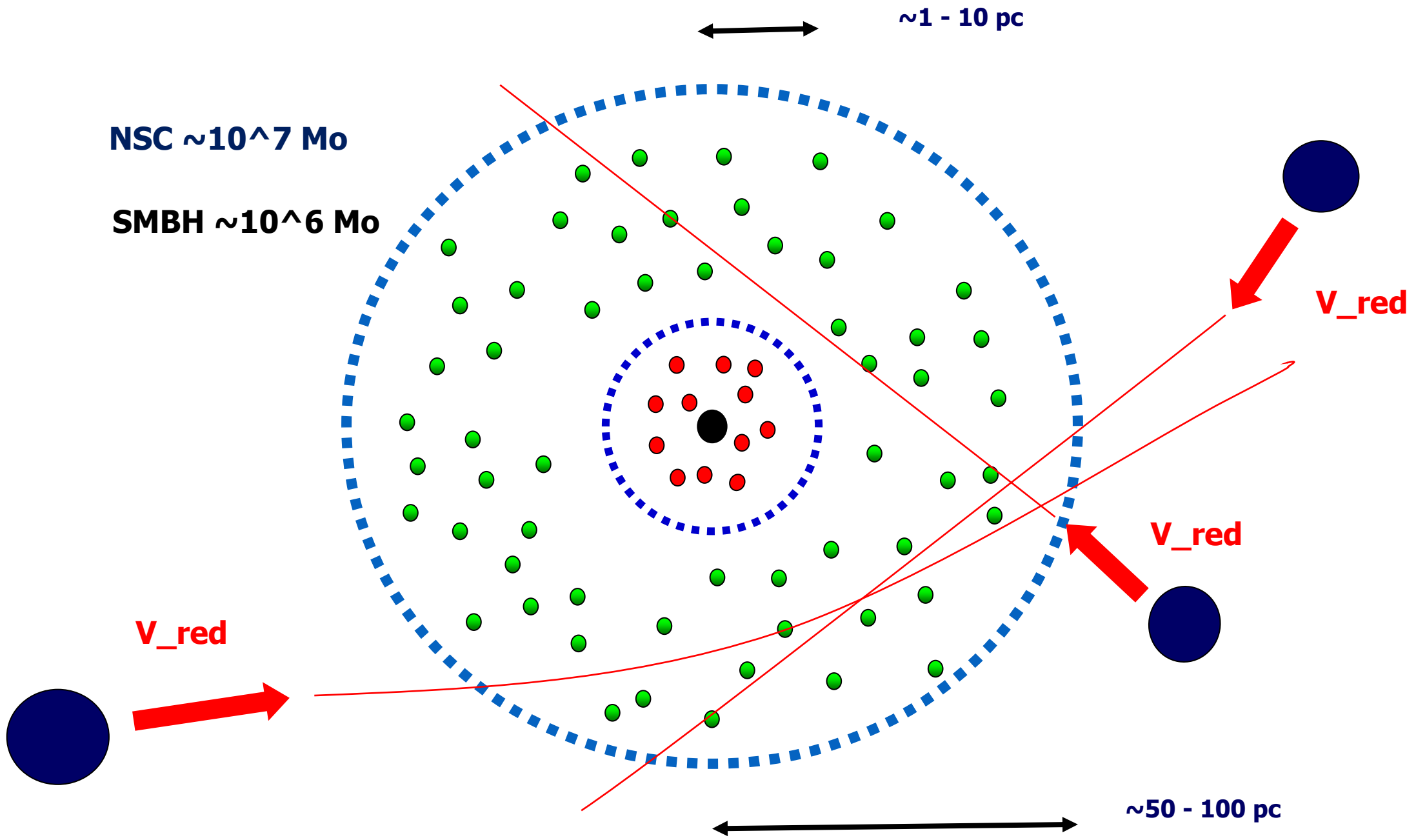
~1 - 10 pc
NSC ~10^7 Mo
SMBH ~10^6 Mo
V_red
V_red
V_red
~50 - 100 pc

https://www.tng-project.org

-The TNG Collaboration

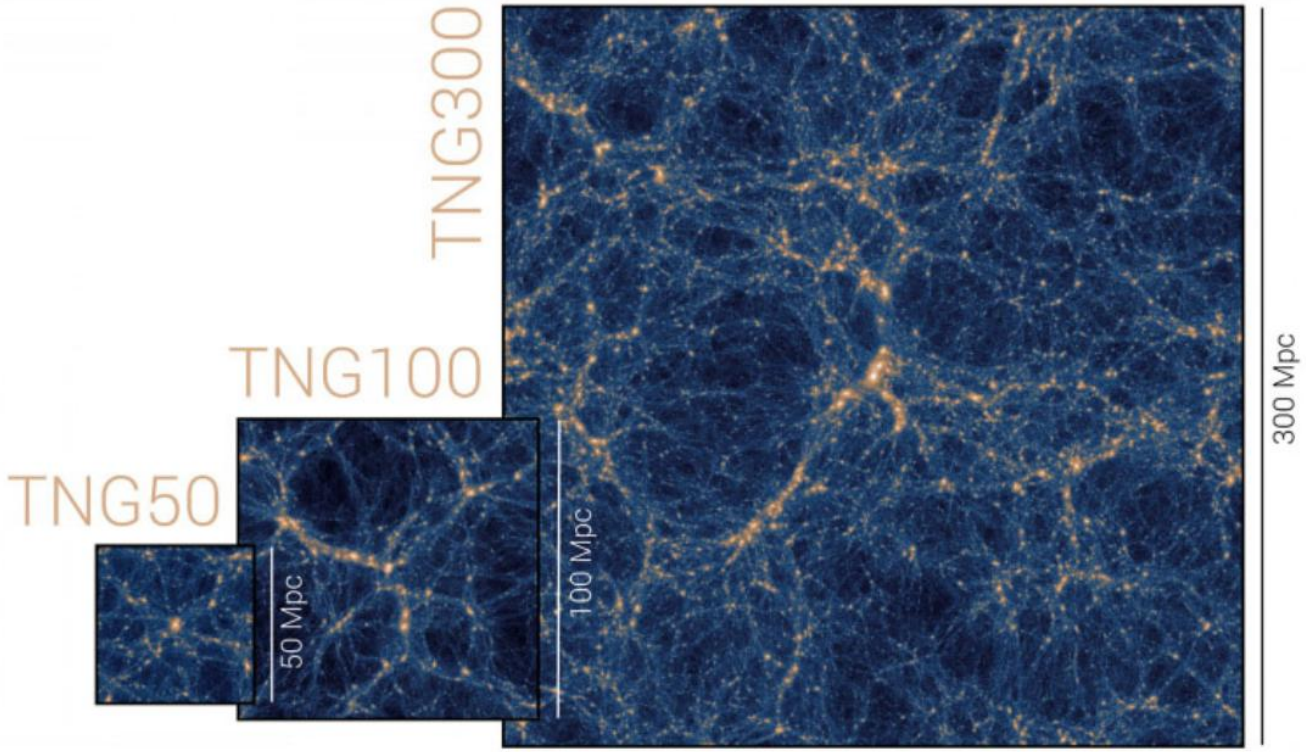

		TNG50	TNG100	TNG300
Volume	$[\mathrm{Mpc}^3]$	51.7^3	110.7^3	302.6^3
L_{box}	$[\mathrm{Mpc}/h]$	35	75	205
N_{GAS}	-	2160^3	1820^3	2500^3
N_{DM}	-	2160^3	1820^3	2500^3
N_{TR}	-	2160^3	2×1820^3	2500^3
m_{baryon}	$[\mathrm{M}_\odot]$	8.5×10^4	1.4×10^6	1.1×10^7
m_{DM}	$[\mathrm{M}_\odot]$	4.5×10^5	7.5×10^6	5.9×10^7
$\epsilon_{\mathrm{gas,min}}$	[pc]	74	185	370
$\epsilon_{\mathrm{DM},\star}$	[pc]	288	740	1480

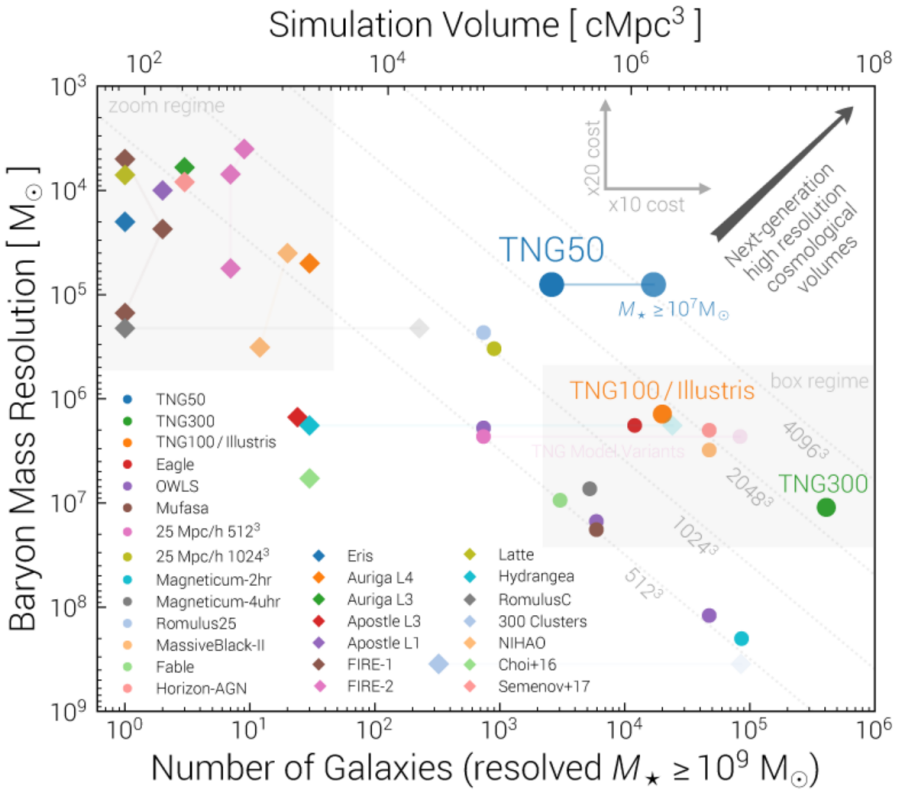

Volker Springel

Heidelberg Institute for Theoretical Studies ➔ MPA

PI: Overall TNG Project

Lars Hernquist

Harvard University

Milky Way and Andromeda analogs from the TNG50 simulation

Annalisa Pillepich[1,⋆], Diego Sotillo-Ramos[1], Rahul Ramesh[2], Dylan Nelson[2], Christoph Engler[1]
Vicente Rodriguez-Gomez[3], Martin Fournier[1], Martina Donnari[1], Volker Springel[4], and Lars Hernquist[5]

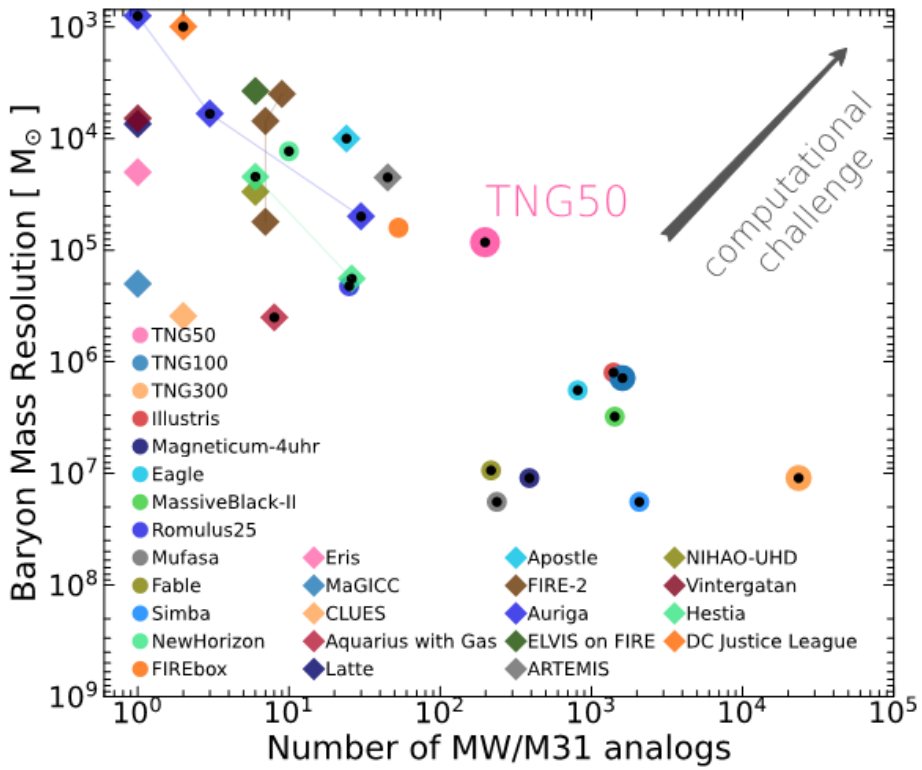

TNG100	2017	AREPO	unif.res.	yes	1606	1.4×10^6
TNG50	**2019**	**AREPO**	**unif.res.**	**yes**	**198**□	8.5×10^4

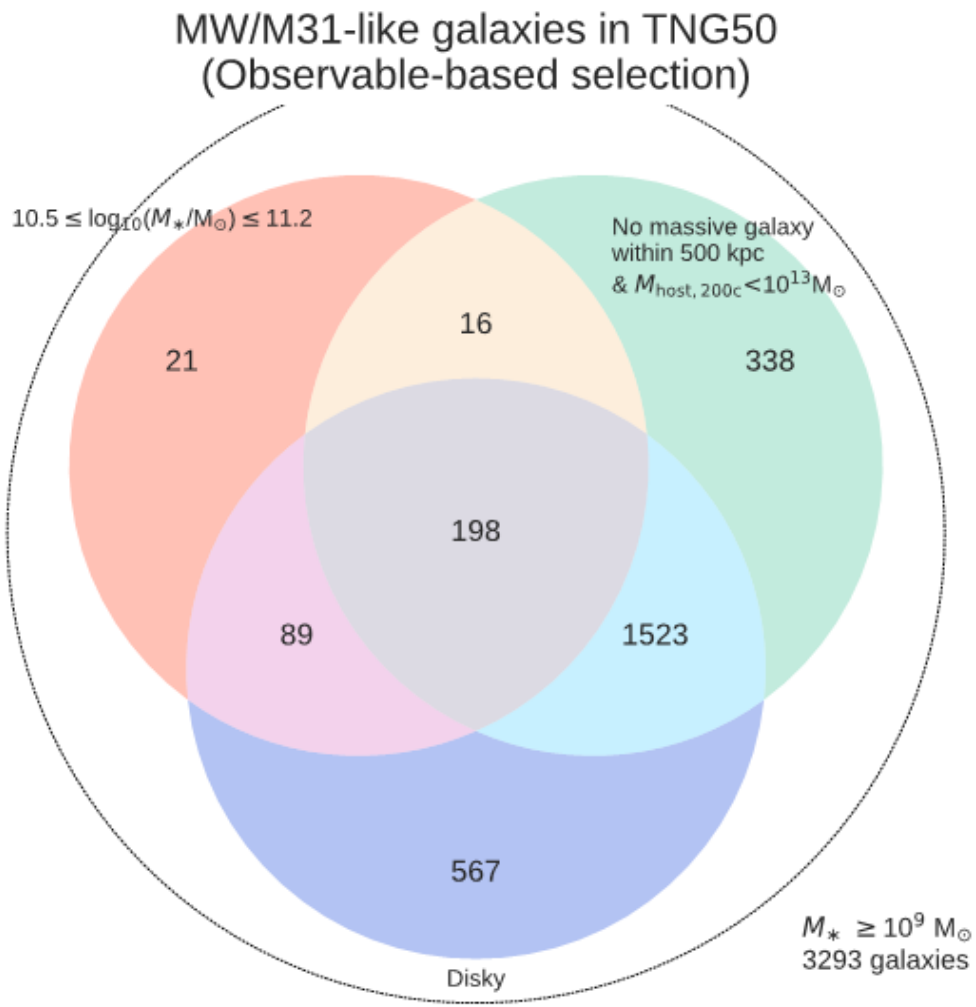

Figure 1. The landscape of ΛCDM cosmological simulations of MW/M31-like galaxies as of 2023. We contrast numerical projects in terms of baryonic mass resolution vs. number of simulated MW/M31 analogs. The TNG50 simulation this paper focuses on (magenta circle) is compared to state-of-the-art cosmological zoom-in simulations (diamonds) and so-called box or uniform-resolution large-volume simulations (circles): this comparison is deliberately similar to that in Fig. 1 of Nelson et al. (2019b) but focuses on MW/M31-

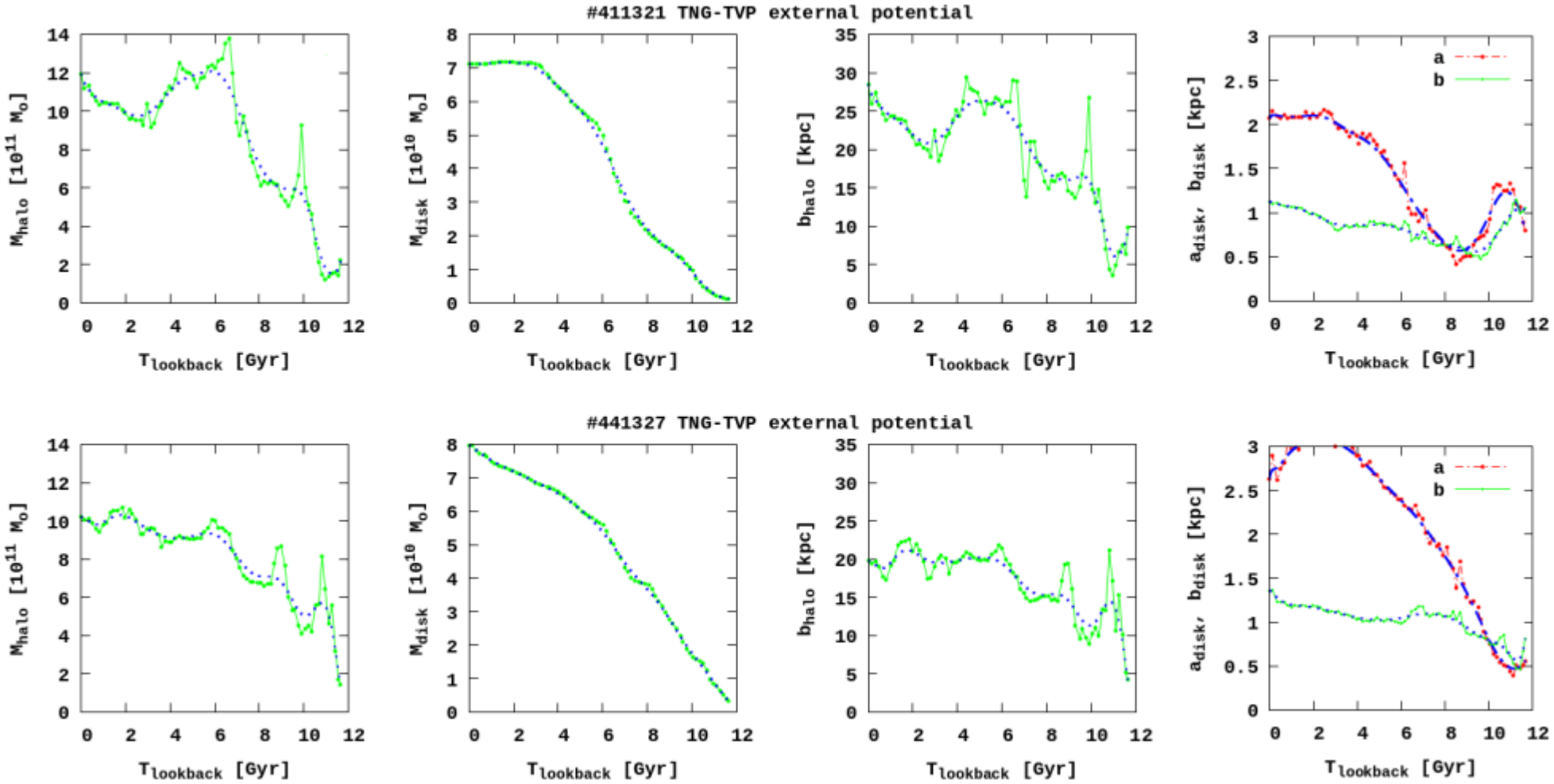

Mardini et al. 2020

https://github.com/Mohammad-Mardini/The-ORIENT

$$\Phi_{\rm tot} = \Phi_{\rm d}(R,z) + \Phi_{\rm h}(R,z) = $$

$$= -\frac{GM_{\rm d}}{\sqrt{R^2 + \left(a_{\rm d} + \sqrt{z^2 + b_{\rm d}^2}\right)^2}} - \frac{GM_{\rm h} \cdot \ln\left(1 + \frac{\sqrt{R^2+z^2}}{b_{\rm h}}\right)}{\sqrt{R^2+z^2}}, \quad (1)$$

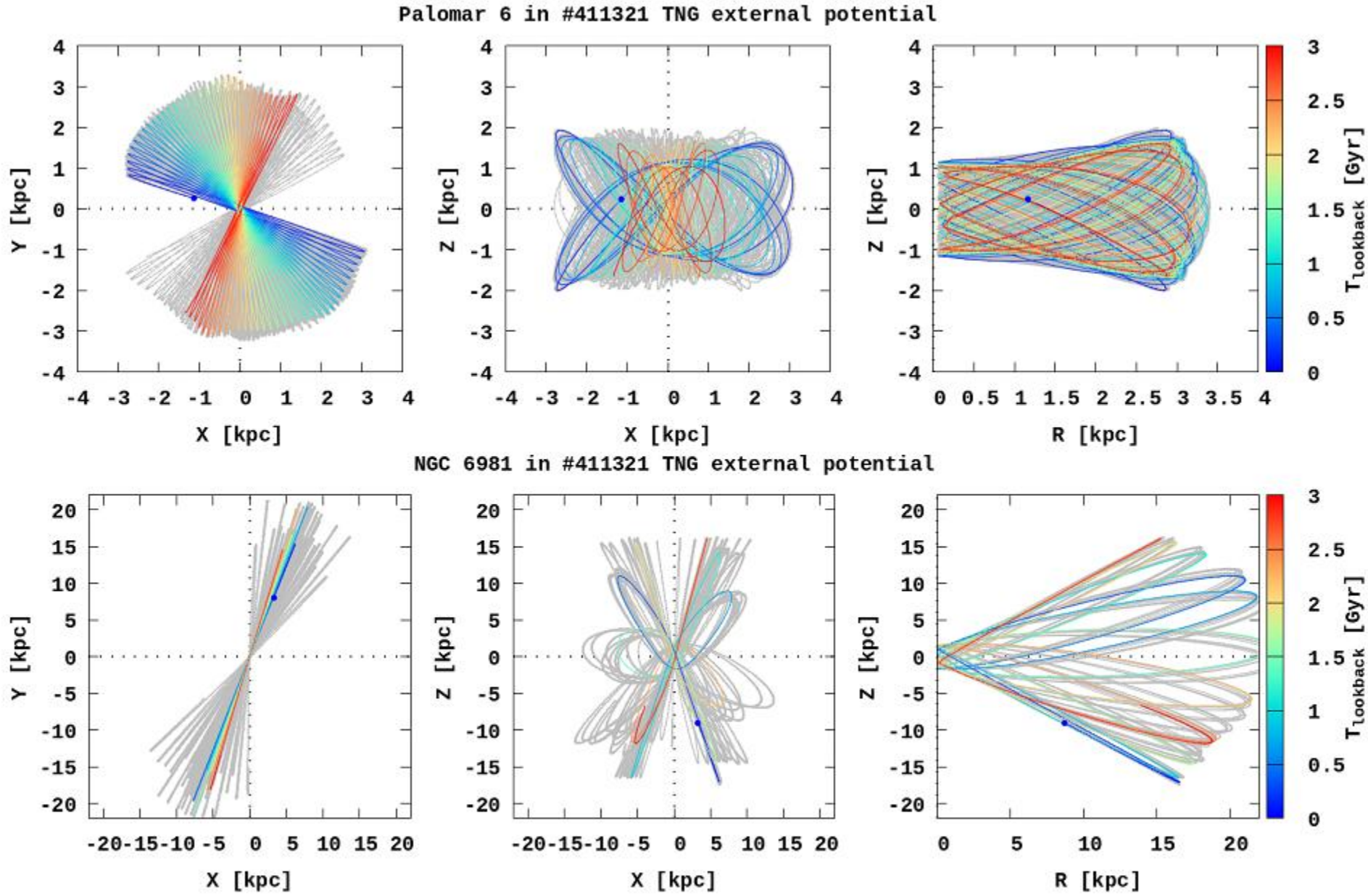

Fig. 1. Orbital evolution of two selected clusters: Pal 6 and NGC 6981. On the plot we show only the first 3 Gyr evolution in #411321 TNG-TVP external potential. The colour-coded line presents the orbit based on catalogue initial positions and velocities. The grey colour represents the orbits for ten different random realisations of initial data.

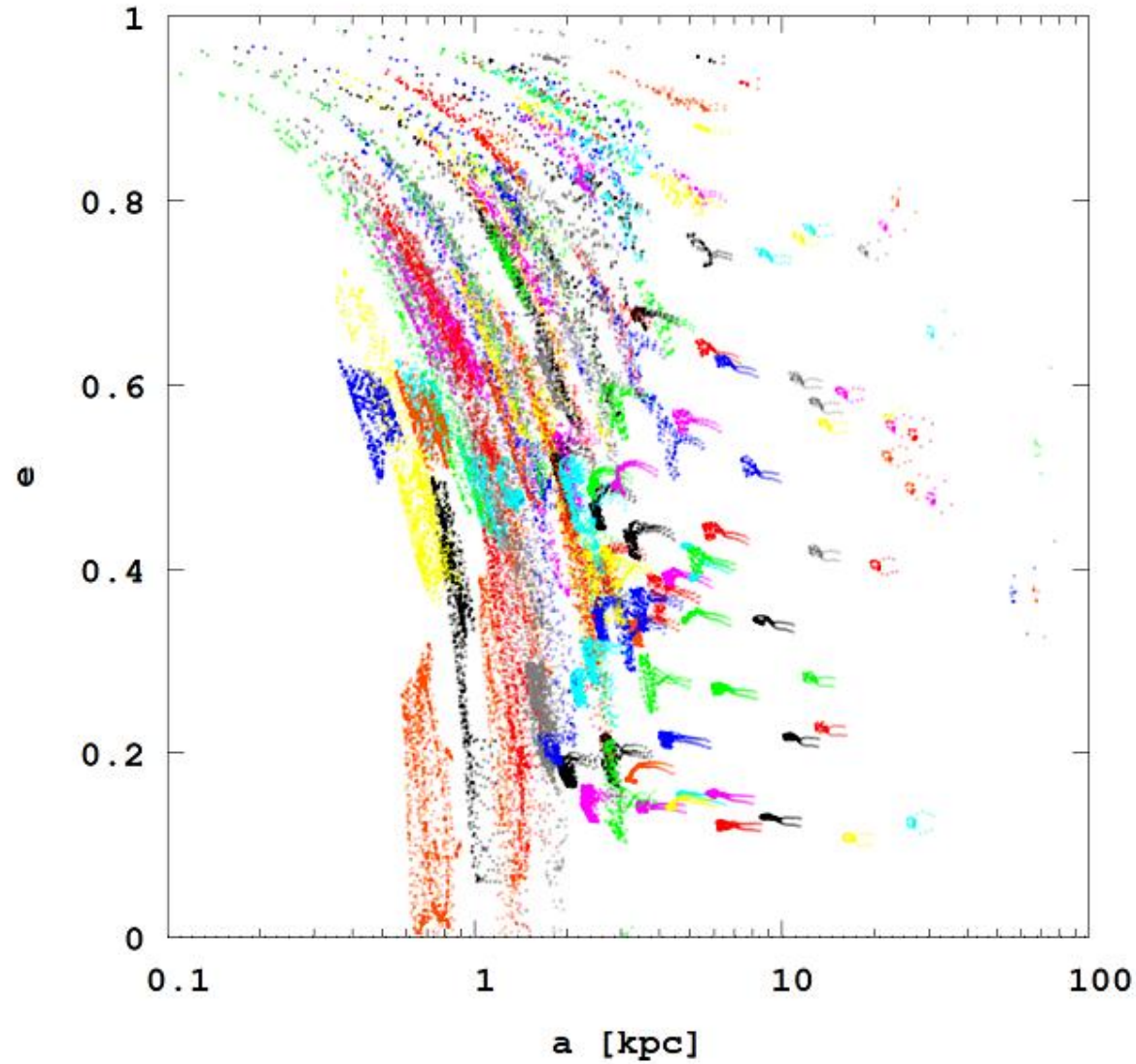

Fig. 6. Evolution of the GC orbital semi-major and eccentricity during the whole backward integration time in the case of 411321 TNG-TVP. The inner GCs (a ≤3 kpc) have more regular and larger eccentricity changes during the evolution. The outer GCs (a >3 kpc) have much smaller eccentricity changes during the whole backward integration time.

$$\frac{dN_{\mathrm{GalC}}(D_{\mathrm{m}})}{dt} = 10^{\mathrm{a}\cdot\lg(D_{\mathrm{m}})+\mathrm{b}},$$

Table 2. Fitting parameters for the interaction rate GC with GalC as a function of the relative distance from the centre for four TNG-TVP external potentials.

Potential	a	b
#411321	3.073 ± 0.588	-5.181 ± 1.205
#411321-m*	3.183 ± 0.609	-5.404 ± 1.247
#441327	3.202 ± 0.584	-5.519 ± 1.187
#451323	2.563 ± 0.328	-3.900 ± 0.670
#462077	2.897 ± 0.594	-4.867 ± 1.218
Mean	2.934 ± 0.524	-4.867 ± 1.070

Notes. * simulations for which additional SMBH mass has been taken into account. This value was not used for the mean calculation.

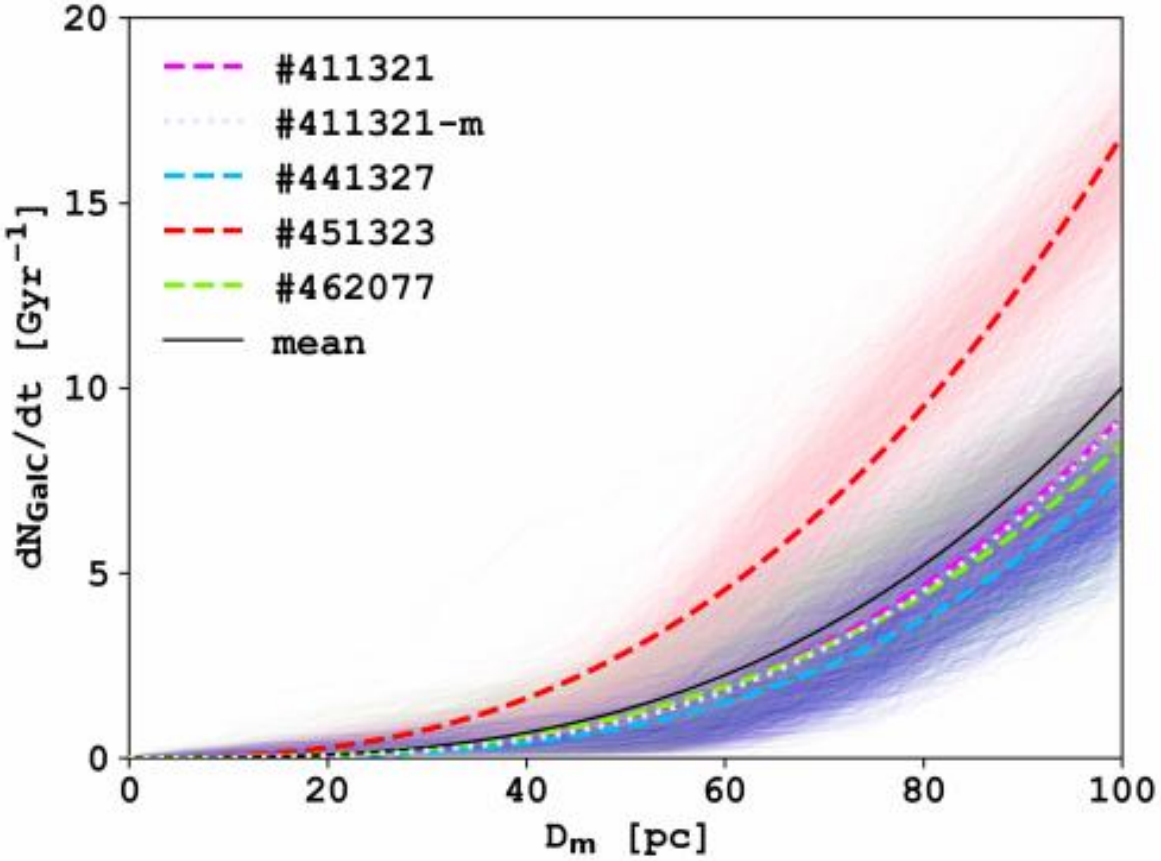

Fig. 2. Interaction rate of the GCs with GalC as a function of the relative distance from the centre for the five TNG-TVP external potentials and 1000 random realisations (thin solid coloured lines). Thick dashed lines are a power-law fit in TNG potentials. The solid black line is a mean fitting line (see Table 2). The pale violet dotted line is a power-law fit for potential #411321-m for which the SMBH mass has been taken into account.

Table 3. Percent of probability of the GCs' interaction with the GalC in all 1000 sets of randomisation for four TNG TVPs.

GC	#411321	#411321-m	#441327	#451323	#462077	Mean
(1)	(2)	(3)	(4)	(5)	(6)	(7)
NGC 6401	100.0	99.9	100.0	100.0	100.0	100.0
Pal 6	100.0	99.6	99.9	100.0	100.0	99.9 ± 0.1
NGC 6681	99.9	99.9	100.0	100.0	100.0	99.9 ± 0.1
NGC 6712	99.9	100.0	99.9	99.8	100.0	99.9 ± 0.1
NGC 6287	100.0	100.0	100.0	97.0	92.1	97.3 ± 3.7
NGC 6642	99.8	99.8	99.3	100.0	99.5	99.7 ± 0.3
NGC 6981	83.9	84.9	90.2	93.5	87.8	88.9 ± 4.0
HP 1	98.7	99.0	70.7	99.5	83.0	89.9 ± 13.8
NGC 1904	72.4	73.0	73.6	83.2	76.7	76.5 ± 4.8
NGC 362	24.4	27.9	30.7	41.2	12.9	27.3 ± 11.8

Notes. Column (1) – name of a GC. Columns (2)–(6) – interaction probabilities for GCs with the GalC for each TNG-TVP external potential in percent. `#411321-m` – the special potential with the MW SMBH mass. Column (7) – the average probability value with error over all potentials, excluding the `#411321-m` potential.

Table 2. Initial kinematics and physical characteristics at eight billion years lookback time for GCs.

GC	X	Y	Z	V_x	V_y	V_z	E/m	$L_{\rm tot}/M$	M	N	$r_{\rm hm}$	W_0
	pc	pc	pc	km s^{-1}	km s^{-1}	km s^{-1}	10^4 km^2 s^{-2}	10^2 kpc km s^{-1}	10^6 M$_\odot$		pc	
(1)	(2)	(3)	(4)	(5)	(6)	(7)	(8)	(9)	(10)	(11)	(12)	(13)
NGC 6401	-1493	-3213	398	5	-3	-57	-18.8	2.03	1.2	2 249640	6.5	9
Palomar 6	1499	465	-1655	140	51	-81	-18.8	1.14	1.0	1 751 970	3.5	9
NGC 6681	1392	-4638	4243	-0.7	-1	61	-16.6	2.9	1.3	2 265 380	3.0	8
NGC 6642	983	-897	545	-47	54	-117	-21.2	1.1	1.5	2 613 856	4.0	9
NGC 6981	1774	4001	-4943	70	159	-270	-11.5	3.7	1.0	1 742 560	7.0	9
HP 1	-580	242	1859	71	-36	128	-19.5	2.3	1.3	2 265 340	6.0	8

Notes. Column (1) – the GCs names; columns (2) – (4) – initial position in Cartesian Galactocentric frame; columns (5) – (7) – initial velocities in Cartesian Galactocentric frame; column (8) – total specific energy; column(9) – total specific angular momentum; column (10) – initial mass; column (11) – initial number of stars; column (12) – initial radius of half-mass; column (13) – initial concentration of King profile.

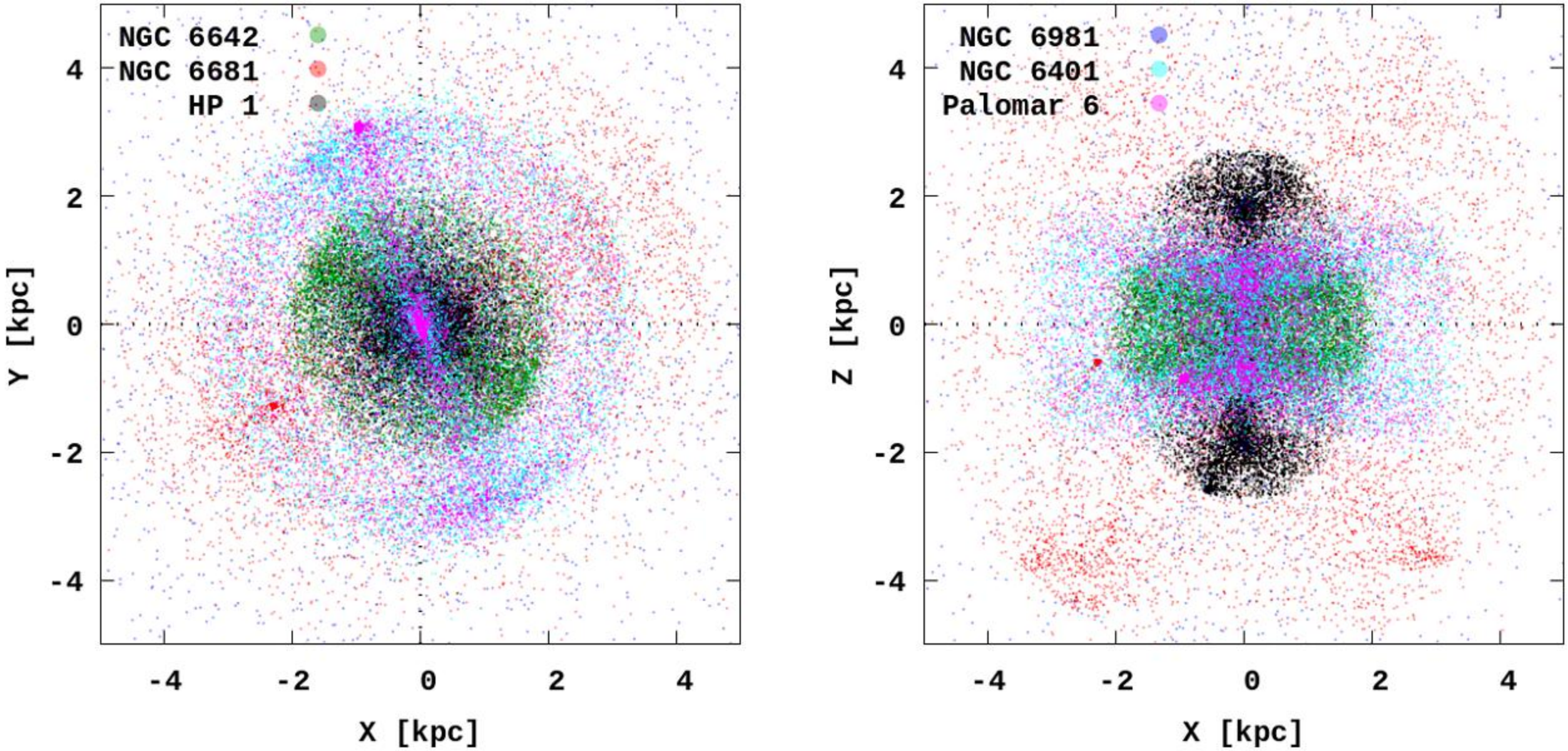

Fig. 8. Positions of the stars for six GCs in the central region of the Galaxy at present time.

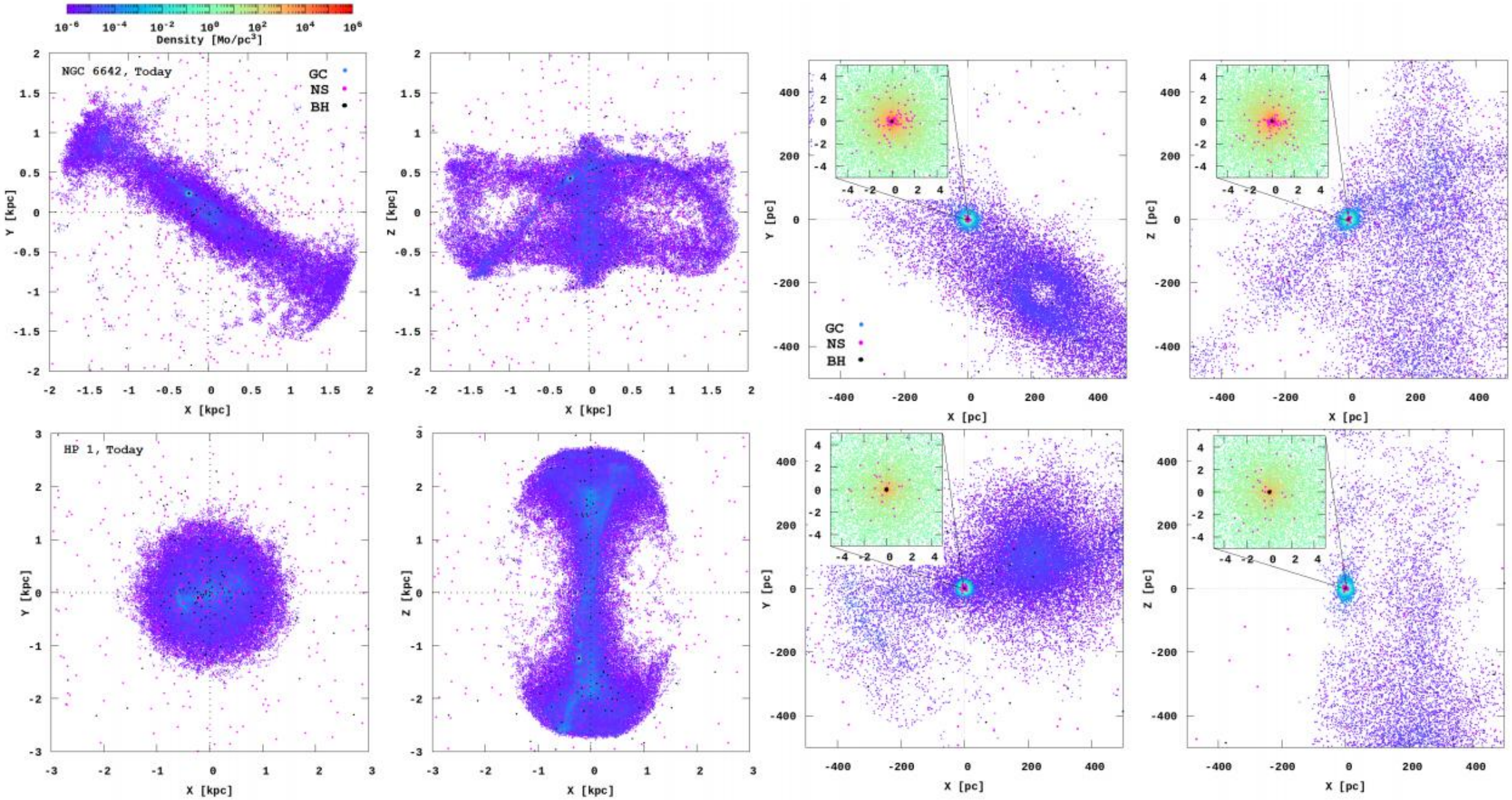

Fig. 9. NGC 6642 and HP 1 clusters today density distributions in 411321 TNG-TVP external potential. The orbital global evolution is present in two planes (X,Y) and (X,Z), *left panels*. GC central part in local frame with the BHs (black dots), NSs (magenta dots) and with detail central area (with box size 10 pc) we present in *two right panels*.

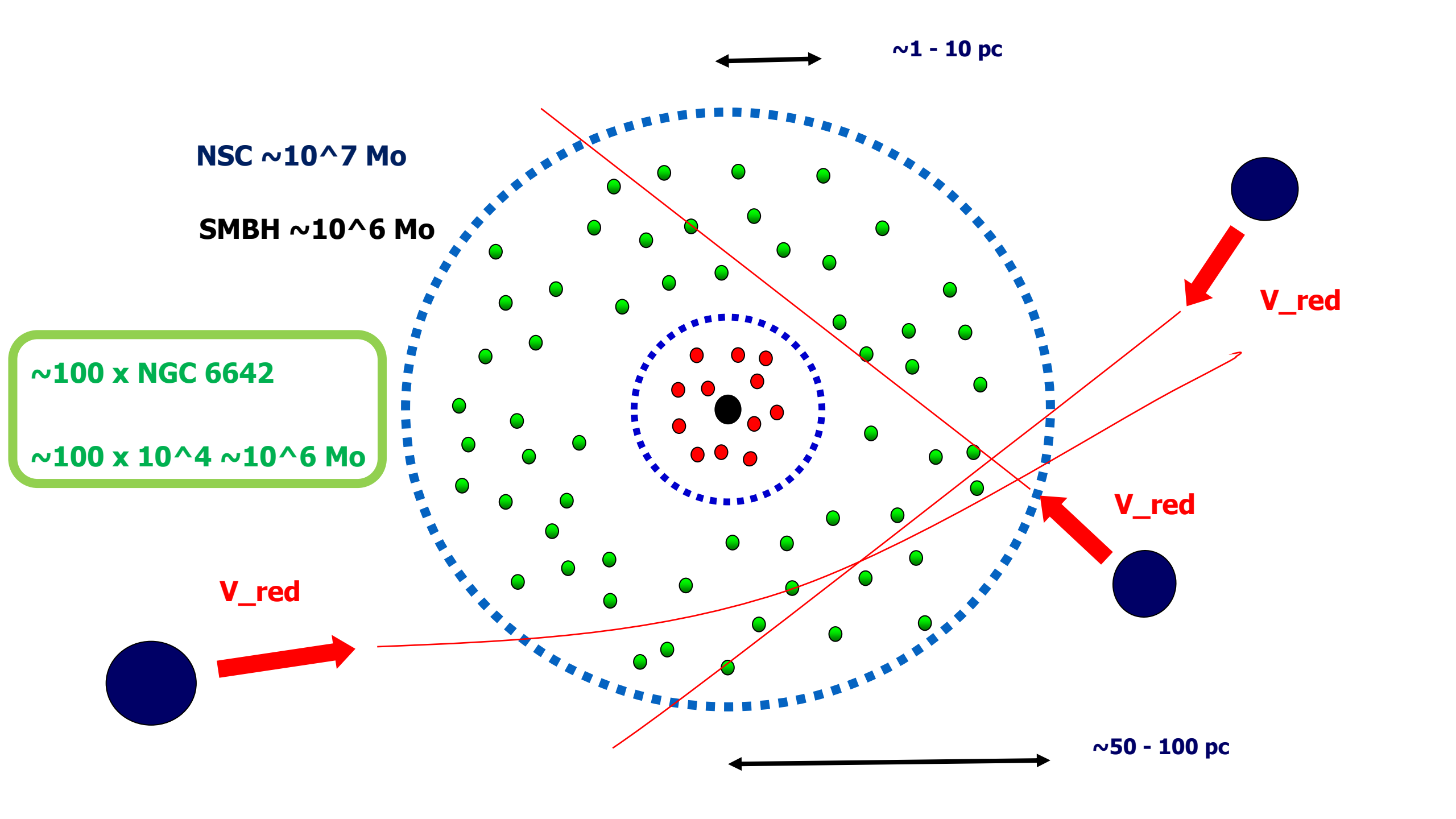
~1 - 10 pc
NSC ~10^7 Mo
SMBH ~10^6 Mo
~100 x NGC 6642
~100 x 10^4 ~10^6 Mo
V_red
V_red
V_red
~50 - 100 pc